# LVRT Scheme of PMSG Wind Power Systems Based on Feedback Linearization

Ki-Hong Kim, Yoon-Cheul Jeung, Dong-Choon Lee, *Member, IEEE*, and Heung-Geun Kim, *Member, IEEE*

***Abstract*—This paper proposes a low-voltage ride-through scheme for the permanent magnet synchronous generator (PMSG) wind power system at the grid voltage sag. The dc-link voltage is controlled by the generator-side converter instead of the grid-side converter (GSC). Considering the nonlinear relationship between the generator speed $\omega_m$ and the dc-link voltage $V_{\rm dc}$, a dc-link voltage controller is designed using a feedback linearization theory. The GSC controls the grid active power for a maximum power point tracking. The validity of this control algorithm has been verified by simulation and experimental results for a reduced-scale PMSG wind turbine simulator.**

***Index Terms*—DC-link voltage, feedback linearization, permanent magnet synchronous generator (PMSG), ride-through, wind power.**

## I. Introduction

AMONG various renewable energy sources, the wind power generation has been concerned as one of the most rapidly growing energy sources. Differently from the doubly fed induction generator (DFIG) wind systems, a direct-drive wind energy conversion system based on permanent magnet synchronous generators (PMSGs) has a lot of advantages such as no gearbox, high power density, high precision, and simple control method, except initial installation costs [1], [2].

As the scale of wind farms becomes larger and larger, the grid connection condition of the wind turbine is more important. Recently, some countries have issued the dedicated grid codes for connecting the wind turbine system to the electric grid [3], [4]. Also, the microgrid and the smart grid have been researched for the efficient power management [5], [6]. However, in these systems, the grid voltage is much fluctuated in comparison with the conventional one. Therefore, a ride-through control of the wind power generation system is needed for the grid abnormal conditions.

The grid codes require the low-voltage ride-through (LVRT) capability of the wind turbine system. For some national grid codes [3], the wind power systems should stay connected to the grid for the grid fault conditions. In the power system where the wind power generation is of a major portion, the grid will experience the power outage if the wind farms trip off. A diagram of the LVRT requirements in which wind turbines should remain connected for voltage sags is shown in Fig. 1 [3].

Several solutions have been proposed for the LVRTs in the variable-speed wind turbine systems. For this purpose, a crowbar system (an external resistor) is connected in the rotor side of the DFIG to absorb the active power during the grid fault [7], [8]. The wind turbine continues its operation to produce the active power, whereas the reactive power or the voltage at the point of common coupling (PCC) is controlled by the grid-side converter (GSC). But, in the case of a weak grid and during a grid fault, the GSC cannot provide sufficient reactive power or voltage support due to its small power capacity and the risk of voltage instability. Also, a static synchronous compensator (STATCOM) has been used to guarantee the uninterrupted operation of a DFIG wind turbine during the grid faults. The reactive power is injected to the grid by the STATCOM that is installed at the PCC [9]–[11]. However, the STATCOM is not used alone for the DFIG ride-through capability since it cannot protect the rotor-side converter (RSC) during a grid fault. On the other hand, it should be used together with the crowbar circuit which protects the RSC from the rotor overcurrent when the grid fault happens.

For the PMSG wind turbine systems, a braking chopper (BC) with the low cost advantage and the simple control performance has been applied for the LVRT [12]–[14]. However, it is difficult to improve the power quality at the output of the wind turbine systems since the BC can just dissipate the power. In other way, the STATCOM has been applied to keep the wind turbine system connected to the grid during grid faults [15]. With this method, the voltage regulation is much improved in the transient state as well as in the steady state. However, the STATCOM has to be used together with the BC.

In the PMSG wind turbine system, the generator is connected to the grid through a full-scale back-to-back pulsewidth modulated (PWM) converters, of which configuration is shown in Fig. 2. Conventionally, the dc-link voltage is controlled by the GSC. However, the GSC may be out of control in the case of the grid voltage sags. At a grid fault, the dc-link voltage is increased excessively since the wind turbine continues to generate the power but the grid cannot absorb the generated power fully.

Manuscript received May 26, 2011; revised August 4, 2011; accepted September 25, 2011. Date of current version February 27, 2012. This work was supported by the Human Resources Development of the Korea Institute of Energy Technology Evaluation and Planning (2007PEPHME040000) grant funded by the Korean Government Ministry of Knowledge Economy. Recommended for publication by Associate Editor P. Rodriguez.

K.-H. Kim is with the LG Electronics Inc., Changwon 641-711, Korea (e-mail: winwin1999@nate.com).

Y.-C. Jeung is with the Department of Electrical Engineering, Yeungnam University, Gyeongsan 712-749, Korea (e-mail: jyclb@naver.com).

D.-C. Lee are with the Department of Electrical Engineering, Yeungnam University, Gyeongbuk 712-749, Korea (e-mail: dclee@yu.ac.kr).

H.-G. Kim is with the Department of Electrical Engineering, Kyungpook National University, Daegu 702-701, Korea (e-mail: kimhg@bh.kyungpook.ac.kr).

Color versions of one or more of the figures in this paper are available online at http://ieeexplore.ieee.org.

Digital Object Identifier 10.1109/TPEL.2011.2171999

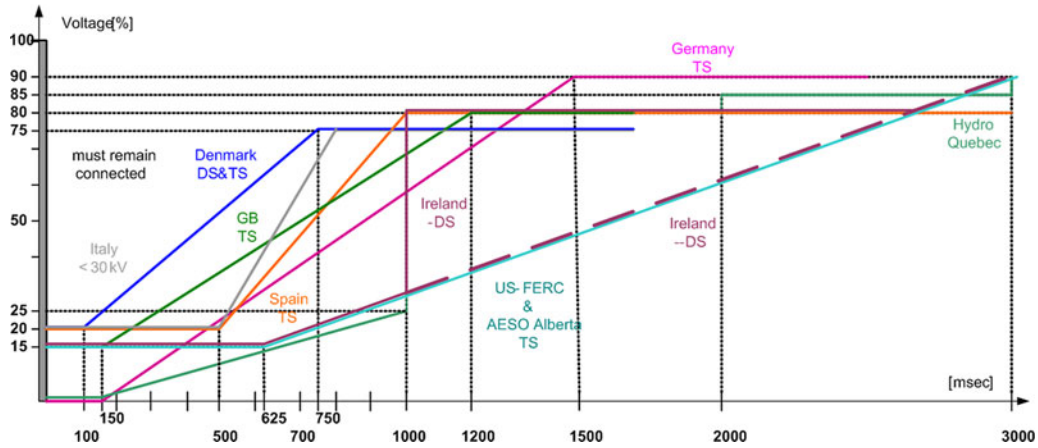


Fig. 1. National grid codes [3].

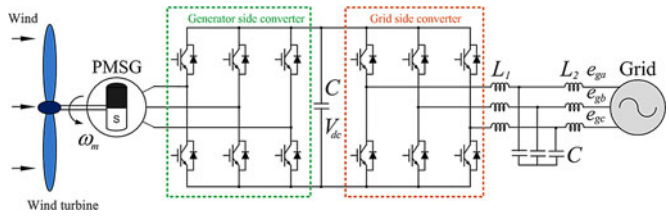


Fig. 2. PMSG wind power system.

A few research results have been suggested that employ the dc-link voltage control strategies by the generator-side converter instead of the GSC [16], [17]. With the exchange of the control roles of the two converters, the dc-link voltage can be controlled to be constant by increasing the generator speed during the grid voltage sag. However, the dc-link voltage response is not so good even though a hybrid adaptive proportional–integral (PI) controller is used based on the power and energy relationship [17]. On the other hand, a linearization technique using an input–output feedback has been applied to various areas such as the dc-link voltage control of PWM converters [18] and the output voltage control of three-phase uninterruptible power system (UPS) inverters [19] for the high dynamic responses. This feedback linearization technique has been applied to the dc-link voltage control for the PMSG wind turbine system in [20]. This paper is the extended version of it, including experimental results.

In the first place, a nonlinear relationship between the generator speed and the dc-link voltage is derived, where the dc-link voltage is chosen as output. Then, by applying the feedback linearization, a linearized system is obtained and then the dc-link voltage controller can be designed by the classical linear control theory. In the meanwhile, the power of the PMSG is controlled by the GSC. The GSC dual current controllers in the positive- and negative-sequence reference frames are employed for grid unbalanced conditions. The validity of the control algorithm has been verified by simulation and experiment results for the PMSG wind power system.

## II. PMSG Wind Power Systems

### A. Modeling of Wind Turbines

The output power of wind turbine $P_t$ is formulated as [21]

$$P_t = \frac{1}{2}\rho A C_p\,(\lambda, \beta)\; v_{\text{wind}}^3 \tag{1}$$

where $\rho$ is the air density (kg/m$^3$), $A$ is the blade swept area (m$^2$), $C_p\,(\lambda, \beta)$ is the power conversion coefficient, and $v_{\text{wind}}$ is the wind speed (m/s).

The power conversion coefficient is a function of the tip-speed ratio (TSR, $\lambda$) and the pitch angle $\beta$, in which the TSR is defined as [22]

$$\lambda = \frac{\omega_m R}{v_{\text{wind}}} \tag{2}$$

where $R$ is the radius of the blade and $\omega_m$ is the rotational speed.

The wind turbine is characterized by $(P_t$–$\omega_m)$ and $(C_p$–$\lambda)$ curves as illustrated in Fig. 3. The turbine power is determined by the power conversion coefficient and the TSR if the swept area, air density, and wind speed are constant.

The power conversion coefficient and the TSR depend on the aerodynamic characteristics of the wind turbine. From Fig. 3(b), the maximum turbine power is found at a point of $\lambda_{\text{opt}}$ and $C_{p\max}$.

### B. Modeling of PMSG

Fig. 4 shows the $d$–$q$ equivalent circuits of the PMSG. The voltage equations of the PMSG are expressed in the synchronous $d$–$q$ coordinates as [22]–[25]

$$v_{ds} = R_s i_{ds} + L_s \frac{di_{ds}}{dt} - \omega_r L_d i_{qs} \tag{3}$$

$$v_{qs} = R_s i_{qs} + L_s \frac{di_{qs}}{dt} + \omega_r L_q i_{ds} + \omega_r \lambda_f \tag{4}$$

where $v_{\text{ds}}$ and $v_{\text{qs}}$ are the $d$- and $q$-axes stator voltages, $i_{\text{ds}}$ and $i_{\text{qs}}$ are the $d$- and $q$-axes stator currents, $R_s$ and $L_s$ are the stator resistance and inductance, $L_d$ and $L_q$ are the $d$- and $q$-axes inductance, $\lambda_f$ is the magnetic flux, and $\omega_r$ is the electrical angular speed.

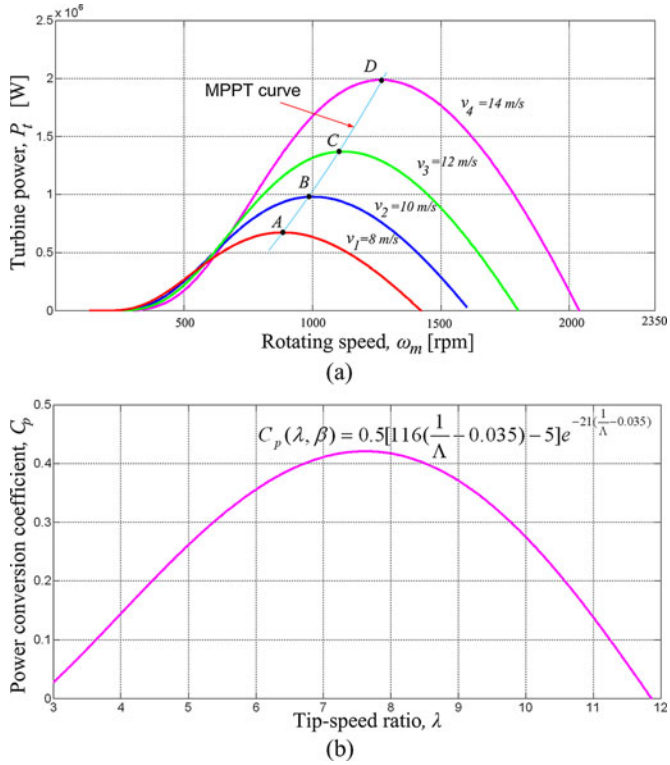


Fig. 3. Wind turbine characteristics. (a) $P_t - \omega_m$ curve. (b) $C_p - \lambda$ curve.

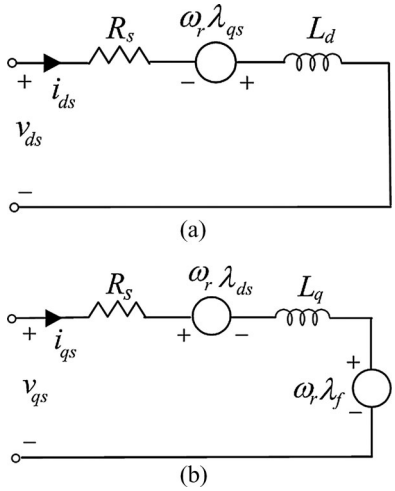


Fig. 4. Equivalent circuits of a PMSG. (a) *d*-axis. (b) *q*-axis.

For the generator with surface-mounted permanent magnets, *d*- and *q*-axes inductances are the same ($L_d = L_q$). Then, the electromagnetic torque $T_e$ is expressed as

$$T_e = \frac{3}{2}\frac{p}{2}\lambda_f i_{qs} \tag{5}$$

where *p* is the number of poles.

## III. Generator Control for Constant DC-Link Voltage

### A. Nonlinear Modeling

The operation of the GSC is directly affected by grid voltage sags, where the power delivered to the grid is restricted. In this duration, the wind turbine and generator keep operating as if it is in normal condition. Therefore, in the dc-link, power delivered from the generator side may increase the dc-link voltage excessively high. Differently from the conventional control of the ac/dc converter, the dc-link voltage for back-to-back converters is controlled by the generator-side converter.

To design the dc-link voltage controller, the dynamic characteristics of wind turbines in the PMSG wind power system are considered. Neglecting the converter loss, the generator power and the DC-link capacitor power can be expressed as

$$P_g = P_t - J\omega_m \frac{d\omega_m}{dt} - P_{g.\text{loss}} \tag{6}$$

$$P_{\text{cap}} = CV_{\text{dc}}\frac{dV_{\text{dc}}}{dt} = P_g - P_{\text{grid}} \tag{7}$$

where $J$ is the moment of inertia, $P_g$ is the generator power, $P_{\text{grid}}$ is the grid power, $P_{g\cdot\text{loss}}$ is the generator loss, $P_{\text{cap}}$ is the dc-link capacitor power, $V_{\text{dc}}$ is the dc-link voltage, and $C$ is the dc-link capacitor.

From (6) and (7), a dynamic equation for the PMSG wind turbine system is expressed as

$$CV_{\text{dc}}\frac{dV_{\text{dc}}}{dt} = \frac{1}{2}\rho AC_p\left(\frac{R}{\lambda}\right)^3\omega_m^3 - J\omega_m\frac{d\omega_m}{dt} - P_{g.\text{loss}} - P_{\text{grid}}. \tag{8}$$

Equation (8) shows a nonlinear relation between $V_{\text{dc}}$ and $\omega_m$. This nonlinear equation can be linearized using a feedback linearization theory, which will be described in the next section.

### B. Feedback Linearization

A single-input and single-output nonlinear system is expressed as [26]

$$\dot{x} = f(x) + g(x)u \tag{9}$$

$$y = h(x) \tag{10}$$

where $x$ is the state vector, $u$ is the control input, $y$ is the output, $f$ and $g$ are the smooth vector fields, and $h$ is the smooth scalar function.

The nonlinear equations in (6) and (7) are expressed in the form of (9) as follows:

$$\begin{bmatrix}\dot{V}_{\text{dc}}\\ \dot{\omega}_m\end{bmatrix} = \begin{bmatrix}-\frac{1}{CV_{\text{dc}}}P_{\text{grid}}\\ \frac{1}{J\omega_m}P_t - \frac{1}{J\omega_m}P_{g.\text{loss}}\end{bmatrix} + \begin{bmatrix}\frac{1}{CV_{\text{dc}}}\\ -\frac{1}{J\omega_m}\end{bmatrix}\cdot P_g. \tag{11}$$

Here, the dc-link voltage $V_{\text{dc}}$ is selected as an output. For the linearization, a relation between input and output should be delivered. So, the output $y$ in (10) is differentiated as

$$\dot{y} = \nabla h\,(f + g\cdot u) = L_f h\,(x) + L_g h\,(x)\cdot u \tag{12}$$

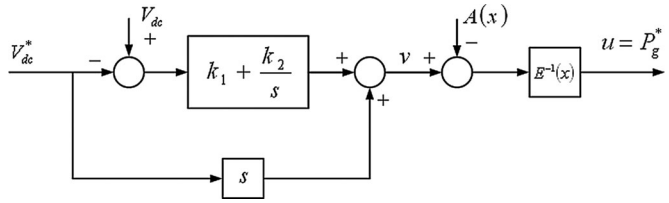


Fig. 5. Control block diagram of the proposed nonlinear dc-link voltage.

where $L_f h(x)$ and $L_g h(x)$ represent Lie derivatives of $h(x)$ with respect to $f(x)$ and $g(x)$, respectively. The Lie derivative is defined as [26]

$$L_f h = \nabla h f = \frac{\partial h}{\partial x} \cdot f. \tag{13}$$

If $L_f h$ and $L_g h$ are replaced to $A(x)$ and $E(x)$, the output of the system is obtained as

$$\dot{y} = A(x) + E(x) \cdot u \tag{14}$$

where $A(x) = -(1/CV_{\rm dc})P_{\rm grid}$, $E(x) = (1/CV_{\rm dc})$.

If a control input $u$ is chosen as

$$u = E^{-1}(x)[-A(x) + v] \tag{15}$$

where $v$ is the equivalent control input to be specified, the resultant dynamics become linear as

$$\dot{y} = v. \tag{16}$$

To eliminate the tracking error in the presence of parameter variations, the new control input with an integral control is given by [18], [19]

$$v = \dot{y}_{\rm ref} - k_1 e - k_2 \int e\, dt \tag{17}$$

where $e = y - y_{\rm ref}$, $y_{\rm ref}$ is the tracking reference, and $k_1$ and $k_2$ are the controller gains.

The controller gains are determined by a pole placement technique [18], [19].

The block diagram of the proposed nonlinear dc-link voltage control is shown in Fig. 5. Unlikely the conventional method, the generator power reference is produced through the dc-link voltage controller instead of the maximum power point tracking (MPPT) controller. The control structure of the generator-side converter consisting of the outer power control loop and the inner current control loop is illustrated in Fig. 6.

## IV. Control of Grid-Side Converters for MPPT

### A. Power Reference

If the air density and blade swept area are invariable, the power of wind turbines depends on the TSR and the turbine speed. The maximum power of the wind turbine is calculated with the maximum power conversion coefficient $C_{p\max}$ and the optimal TSR $\lambda_{\rm opt}$ as

$$P_t = \frac{1}{2}\rho A C_{p\max}\left(\frac{\omega_m R}{\lambda_{\rm opt}}\right)^3 = K_{\rm opt}\cdot\omega_m^3 \tag{18}$$

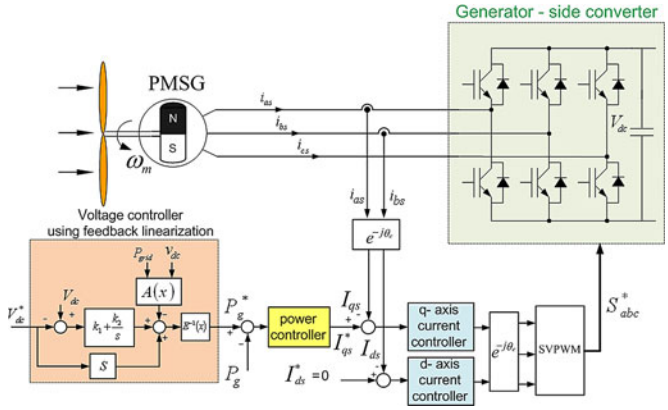


Fig. 6. Control block diagram of the generator-side converter.

where $K_{\rm opt} = \frac{1}{2}\rho A C_{p\max}\left(\frac{R}{\lambda_{\rm opt}}\right)^3$.

From (8) and (18), the grid power reference is given by

$$P_{\rm grid}^* = K_{\rm opt}\cdot\omega_m^3 - J\omega_m\frac{d\omega_m}{dt} - P_{g.\rm loss} - CV_{\rm dc}\frac{dV_{\rm dc}}{dt}. \tag{19}$$

As can be seen in (19), the grid power reference $P_{\rm grid}^*$ is obtained from the inertial power, the generator loss, the dc-link capacitor power, and the generator power reference obtained by applying the MPPT method from the wind turbines.

### B. Current Control Under Unbalanced Grid Voltage

In unbalanced grid voltage conditions, the positive-sequence voltage component in the stationery reference frame is expressed as [27]

$$\begin{bmatrix} e_{ga}^+ \\ e_{gb}^+ \\ e_{gc}^+ \end{bmatrix} = \begin{bmatrix} \frac{1}{3}\left(e_{ga} - \frac{e_{gb}}{2} - \frac{e_{gc}}{2}\right) - \frac{1}{j2\sqrt{3}}(e_{ga} - e_{gc}) \\ \frac{1}{3}\left(e_{gb} - \frac{e_{gc}}{2} - \frac{e_{ga}}{2}\right) - \frac{1}{j2\sqrt{3}}(e_{gc} - e_{ga}) \\ \frac{1}{3}\left(e_{gc} - \frac{e_{ga}}{2} - \frac{e_{gb}}{2}\right) - \frac{1}{j2\sqrt{3}}(e_{ga} - e_{gb}) \end{bmatrix} \tag{20}$$

where $e_{\rm ga}$, $e_{\rm gb}$, $e_{\rm gc}$ and $e_{\rm ga}^+$, $e_{\rm gb}^+$, $e_{\rm gc}^+$ are the instantaneous grid voltages and the positive-sequence components, respectively. The $j$ in (20) means the phase shift of 90°, which is obtained by using all-pass filters [27]. The $d$-axis voltage which is calculated from the positive-sequence component of the grid voltages is controlled to be zero, from which the reference phase angle for control is determined.

The apparent power delivered to the grid under unbalanced conditions is expressed in terms of the positive- and negative-sequence components as [28]

$$S = 1.5\left(e^{j\omega t}e_{dq}^+ + e^{j(-\omega)t}e_{dq}^-\right)\left(e^{j\omega t}i_{dq}^+ + e^{j(-\omega)t}i_{dq}^-\right)^* \tag{21}$$

where the superscript "$*$" represents a complex conjugate value, and the superscripts "$+$" and "$-$" are the positive- and negative-sequence components, respectively.

Thus, the apparent power is divided into the real power *p(t)* and the reactive power *q(t)* [28]

$$p(t) = P_0 + P_{c2}\cos(2\omega t) + P_{s2}\sin(2\omega t) \quad (22)$$

$$q(t) = Q_0 + Q_{c2}\cos(2\omega t) + Q_{s2}\sin(2\omega t) \quad (23)$$

where

$$\begin{aligned}
P_0 &= 1.5(E_d^+ I_d^+ + E_q^+ I_q^+ + E_d^- I_d^- + E_q^- I_q^-)\\
P_{c2} &= 1.5(E_d^+ I_d^- + E_q^+ I_q^- + E_d^- I_d^+ + E_q^- I_q^+)\\
P_{s2} &= 1.5(E_d^+ I_q^- - E_q^+ I_d^- - E_d^- I_q^+ + E_q^- I_d^+)\\
Q_0 &= 1.5(-E_d^+ I_q^+ + E_q^+ I_d^+ - E_d^- I_q^- + E_q^- I_d^-)\\
Q_{c2} &= 1.5(-E_d^+ I_q^- + E_q^+ I_d^- - E_d^- I_q^+ + E_q^- I_d^+)\\
Q_{s2} &= 1.5(E_d^+ I_d^- + E_q^+ I_q^- - E_d^- I_d^+ - E_q^- I_q^+).
\end{aligned}$$

From (22) and (23), the power ($P_0$, $Q_0$, $P_{s2}$, $P_{c2}$) can be represented in a matrix form as

$$\begin{bmatrix} P_0 \\ Q_0 \\ P_{s2} \\ P_{c2} \end{bmatrix} = \frac{3}{2}\begin{bmatrix} E_d^+ & E_q^+ & E_d^- & E_q^- \\ E_q^+ & -E_d^+ & E_q^- & -E_d^- \\ E_q^- & -E_d^- & -E_q^+ & E_d^+ \\ E_d^- & E_q^- & E_d^+ & E_q^+ \end{bmatrix}\begin{bmatrix} I_d^+(t) \\ I_q^+(t) \\ I_d^-(t) \\ I_q^-(t) \end{bmatrix}. \quad (24)$$

The second-order components of power ($P_{c2}$, $P_{s2}$) due to the unbalanced grid voltage fluctuate not only the dc-link capacitor power but also the real power delivered to the grid. These two components should be controlled to zero in order to eliminate the power fluctuations. The real power reference $P_0^*$ is obtained in (19). The reactive power reference $Q_0^*$ can be determined from unity power factor operation or other grid requirements. Therefore, the positive- and negative-sequence components of the current references are expressed as

$$\begin{bmatrix} I_d^+(t)^* \\ I_q^+(t)^* \\ I_d^-(t)^* \\ I_q^-(t)^* \end{bmatrix} = \frac{2}{3}\begin{bmatrix} E_d^+ & E_q^+ & E_d^- & E_q^- \\ E_q^+ & -E_d^+ & E_q^- & -E_d^- \\ E_q^- & -E_d^- & -E_q^+ & E_d^+ \\ E_d^- & E_q^- & E_d^+ & E_q^+ \end{bmatrix}^{-1}\begin{bmatrix} P_{\text{grid}}^* \\ Q_0^* \\ 0 \\ 0 \end{bmatrix}. \quad (25)$$

The control block diagram of the GSC that includes the dual current controller for positive- and negative-sequence components is shown in Fig. 7 [28].

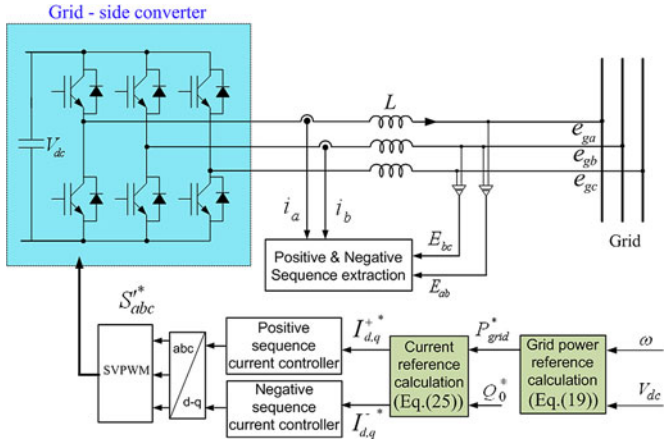


Fig. 7. Control block diagram of the GSC.

## V. Simulation Results

To verify the validity of the proposed algorithm, PSIM simulation has been performed for 2 MW PMSG wind power system. The parameters of the wind turbine are listed in Table I in the Appendix. The dc-link voltage is controlled at 1100 V, the dc-link capacitance is 0.1 F, the switching frequency is 2 kHz, and the grid voltage is 690 $V_{rms}$/60 Hz.

Fig. 8 shows the system performance in the normal grid condition. The wind speed is shown in Fig. 8(a). The generator speed, turbine, generator and grid power, wind turbine and generator torque, and power conversion coefficient are shown from Fig. 8(b)–(e), respectively. In this case, the generator is controlled to keep the dc-link voltage constant, of which variation is less than 1% as shown in Fig. 8(f).

TABLE I
Parameters of Wind Turbine for Simulation

| | |
|---|---|
| Rated power | 2[MW] |
| Air density | 1.225[kg/m$^3$] |
| Blade radius | 45[m] |
| Max. power conv. coeff. | 0.41 |
| Optimal tip-speed ratio | 8.1 |
| Rated wind speed | 13.5[m/s] |

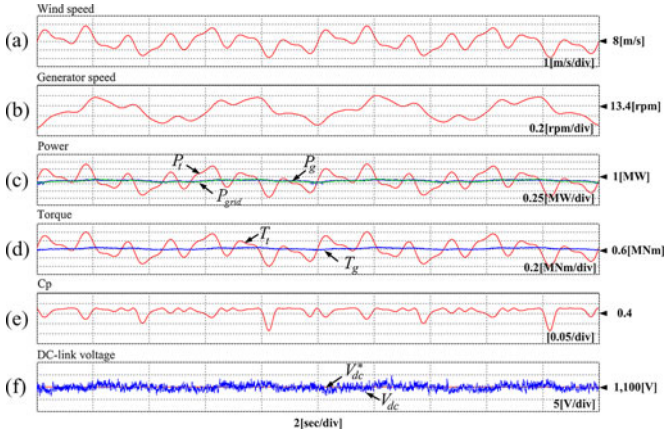


Fig. 8. Wind generation performance for normal grid condition. (a) Wind speed. (b) Generator speed. (c) Turbine, generator, and grid power. (d) Wind turbine and generator torque. (e) Power conversion coefficient. (f) DC-link voltage.

Fig. 9 shows the system performance for a grid unbalanced voltage sag, where the wind speed is assumed to be constant (8 m/s) for easy examination. The fault condition is 50% sag in the grid A-phase voltage for 1.5 s (90 cycles), which is between the point ⓐ to ⓑ as shown in Fig. 9(a). Fig. 9(b) shows the magnified grid voltages for six cycles just before and after fault. The positive- and negative-sequence *d–q* axis voltages are shown in Fig. 9(c). Due to the grid unbalanced voltage sag, the

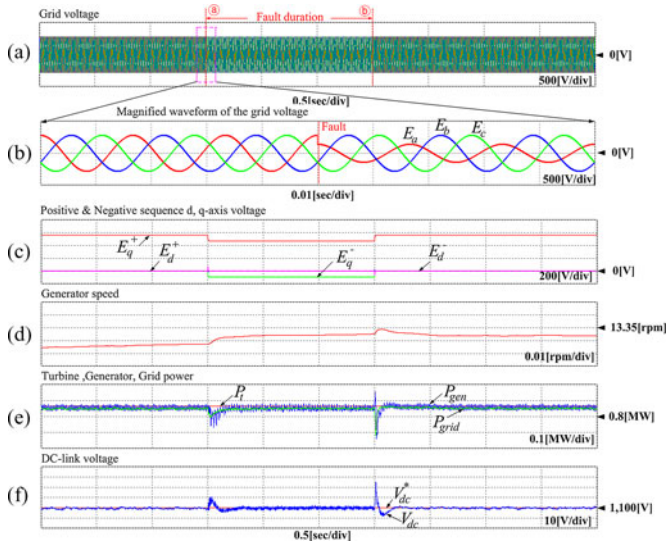


Fig. 9. Wind generation performance for grid phase-A voltage sag (50%). (a) Grid voltage. (b) Magnified waveform of the grid voltage. (c) Positive- and negative-sequence *d–q* axis voltage. (d) Generator speed. (e) Turbine, generator, and grid power. (f) DC-link voltage.

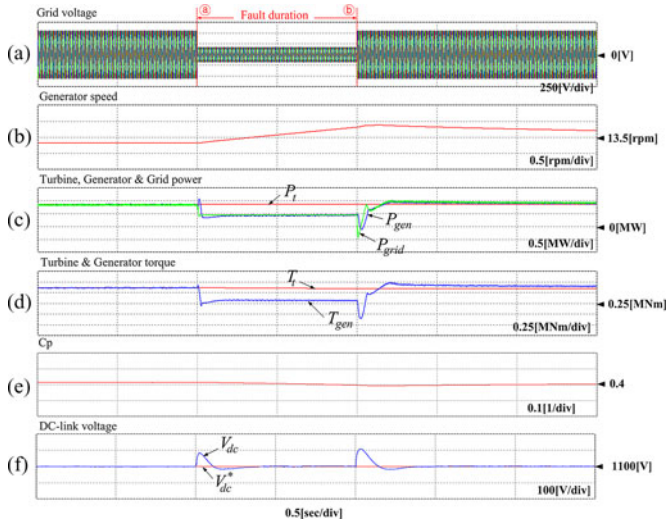


Fig. 10. Wind generation performance for grid balanced voltage sag. (a) Grid voltage. (b) Generator speed. (c) Turbine, generator, and grid power. (d) Turbine and generator torque. (e) Power conversion coefficient. (f) DC-link voltage.

positive-sequence $q$-axis voltage is reduced and the negative-sequence $d$–$q$ voltage components appear. In this voltage event, the variation of the dc-link voltage is controlled within 3%.

For 70% sag of the all grid phase voltages for 1 s, the system performance is shown in Fig. 10.

During the grid fault, the grid and generator power are decreased due to the low grid voltage and the current limitation of the converters as shown in Fig. 10(c) and the generator speed is increased as shown in Fig. 10(b). The turbine power $P_t$ is a little decreased since the turbine speed is changed from the optimal value for the MPPT. However, it looks almost constant just because of scaling. Likewise, the turbine and generator torques are also decreased, which is illustrated in Fig. 10(d), where the turbine torque just looks constant. Fig. 10(e) shows

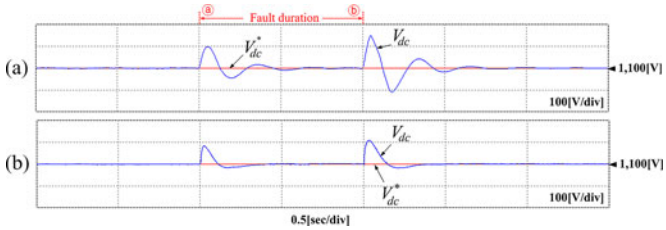


Fig. 11. Performance of dc-link voltage control. (a) PI control. (b) Feedback linearization.

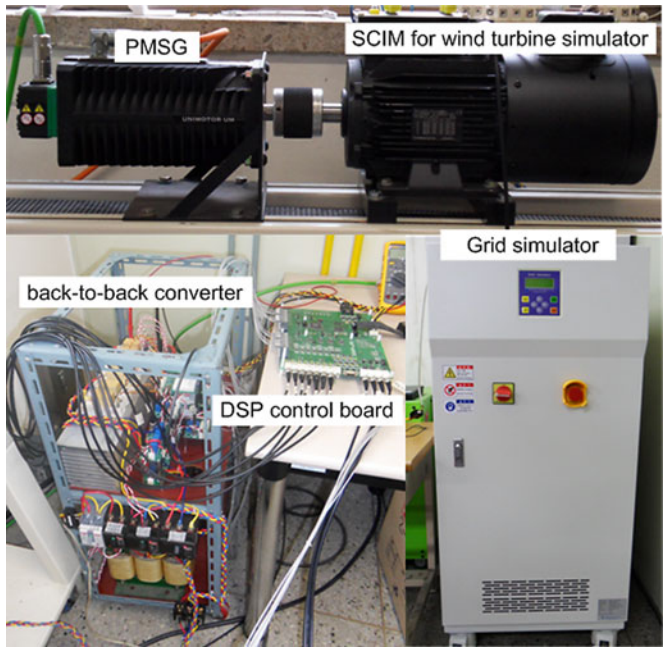


Fig. 12. Layout of experimental setup.

the power conversion coefficient, which is deviated from its maximum value during the fault. Due to the speed change, the $C_p$ is slightly decreased during the fault. Fig. 10(f) shows the dc-link voltage, of which variation is less than 10%.

Fig. 11 shows the dc-link voltage responses for the two controllers: 1) for the PI controllers [29] with $k_P = 14.734$ and $k_I = 833.629$ which are obtained by setting $\xi = 0.707$ and $\omega_n = 80$ rd/s and 2) for the feedback linearization method with $k_1 = 15.3$ and $k_2 = 81.25$ which are determined by assigning the desired poles at $s_{1,2} = -75 \pm j50$. By locating the system poles on the left-half plane, it is guaranteed that the closed-loop control system is stable [18], [30]. The proposed method gives faster transient response and lower overshoot.

## VI. Experimental Results

To demonstrate the validity of the proposed algorithm, the experiment has been carried out for a 2.68 kW PMSG wind power system. The picture of the experimental setup at the laboratory is shown in Fig. 12, where a squirrel-cage induction is used as a turbine simulator. The parameters of the PMSG and wind turbine are listed in Tables II and III in the Appendix, respectively. The dc-link voltage is controlled at 340 V. The

TABLE II
PARAMETERS OF THE PMSG FOR EXPERIMENT

| | |
|---|---|
| Rated power | 2.68 [kW] |
| Voltage/frequency | 220[V]/60[Hz] |
| Rated flux | 0.468[Wb] |
| Rated current | 9.8[Arms] |
| Rated speed | 1200[rpm] |
| Torque constant | 1.72[N·m/A] |
| Moment of inertia | 0.00331[kg·m$^2$] |
| Stator resistance | 0.49 [Ω] |
| Stator inductance | 5.35[mH] |
| Number of poles | 6 |

TABLE III
PARAMETERS OF THE WIND TURBINE FOR EXPERIMENT

| | |
|---|---|
| Rated power | 2.68 [kW] |
| Air density | 1.225 [kg/m$^3$] |
| Blade radius | 0.88 [m] |
| Max. power conv. coeff. | 0.43 |
| Optimal tip-speed ratio | 7.9 |
| Cut-in/cut-out speed | 3 [m/s] / 25 [m/s] |
| Rated wind speed | 16.1 [m/s] |
| Blade inertia | 0.00331 [kg.m$^2$] |

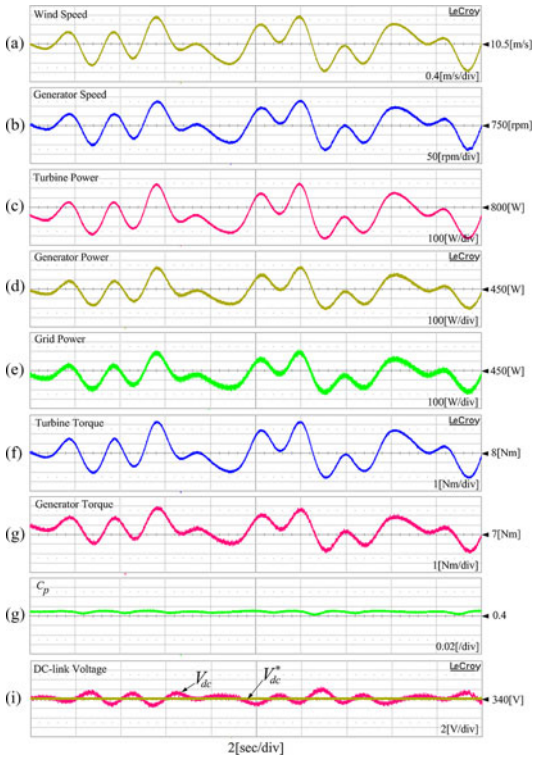


Fig. 13. Wind turbine performance for the grid normal condition. (a) Wind speed. (b) Generator speed. (c) Turbine power. (d) Generator power. (e) Grid power. (f) Turbine torque. (g) Generator torque. (h) Power conversion coefficient. (i) DC-link voltage.

capacitance of the 1650 $\mu$F is used for dc-link capacitor. The switching frequency is 5 kHz. The grid voltage is 220 $V_{\rm rms}$/60 Hz and a 10 kVA] grid simulator is used for a sag generation.

Fig. 13 shows the performance of the PMSG wind power system in the grid normal condition, at the mean wind speed of 10.5 m/s [see Fig. 13(a)]. For the random variation of the wind speed, the generator speed, the wind turbine, the generator power, and the grid power vary as illustrated in Fig. 13(b)–(e), respectively, where the turbine power is proportional to the cube

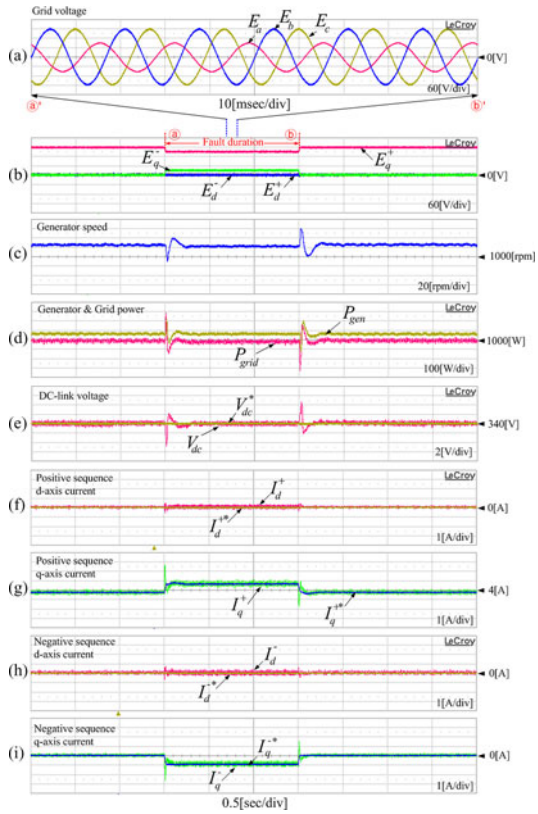


Fig. 14. System performance under A-phase unbalanced voltage drop. (a) Three-phase voltage. (b) Positive and negative $d$–$q$ axis voltage. (c) Generator speed. (d) Generator and grid power. (e) DC-link voltage. (f) Positive-sequence $d$-axis current. (g) Positive-sequence $q$-axis current. (h) Negative-sequence $d$-axis current. (i) Negative-sequence $q$-axis current.

of the wind speed. Also, the turbine and generator torques are shown in Fig. 13(f) and (g), respectively, which are proportional to the square of the wind speed. Fig. 13(h) shows the variation of the power conversion coefficient according to the turbine speed, from which the wind turbine system is seen to track the maximum power point. In this case, the dc-link voltage follows its reference well and is maintained within the variation of 1%, as illustrated in Fig. 13(i).

Fig. 14 shows the system performance for a grid unbalanced voltage sag, where the wind speed is assumed to be constant (11.6 m/s). The fault condition in Fig. 14 is 50% sag of the grid A-phase voltage for 1.5 s (90 cycles), which appears between the point ⓐ to ⓑ. In the middle of this fault duration, a six-cycle voltage waveform is magnified as illustrated in Fig. 14(a), for easier view. The positive- and negative-sequence $d$–$q$ axis voltages are shown in Fig. 14(b). The positive-sequence $q$-axis voltage component is decreased due to the grid unbalanced voltage sag. Fig. 14(e) shows the responses of the dc-link voltage control. The dc-link voltage variation is controlled within 2%. Fig. 14(f)–(i) shows the positive- and negative-sequence $d$–$q$ axis currents of the GSC. The actual currents are well controlled to follow the reference values.

Fig. 15 shows the system performance for grid unbalanced voltage sags which are 30%, 20%, and 10% for A-phase, B-phase, and C-phase voltages, respectively, for 1.5 s, as shown in Fig. 15(a). Fig. 15(c) shows the generator speed and Fig. 15(d) shows the generator and grid power. Fig. 15(f)–(i)

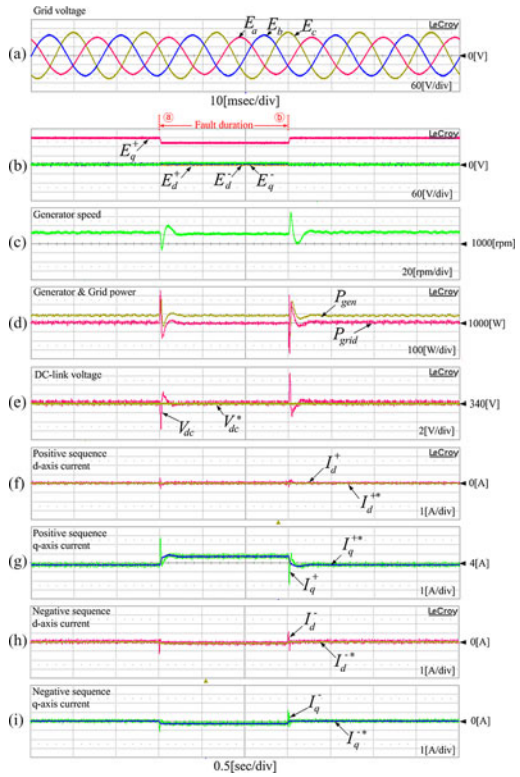


Fig. 15. System performance under three-phase unbalanced voltage drop. (a) Three-phase voltage. (b) Positive and negative $d$–$q$ axis voltage. (c) Generator speed. (d) Generator and grid power. (e) DC-link voltage. (f) Positive-sequence $d$-axis current. (g) Positive-sequence $q$-axis current. (h) Negative-sequence $d$-axis current. (i) Negative-sequence $q$-axis current.

shows the positive- and negative-sequence $d$–$q$ axis currents of the GSC. The actual currents are well controlled to the reference values. In this voltage event, the variation of the dc-link voltage is within 2%.

Fig. 16 shows the system performance in the case that the grid voltages have the balanced sags of 70% which occur between ⓐ to ⓑ in Fig. 16(a). During the fault duration, the generator speed is increased to maintain the dc-link voltage constant as shown in Fig. 16(b). Also, the grid, generator and turbine powers are illustrated in Fig. 16(c) and (d), respectively. Likewise, the generator and turbine torques are shown in Fig. 16(e) and (f), respectively. Fig. 16(g) shows the power conversion coefficient, which is decreased from its maximum value for the fault duration. The decrease of the power conversion coefficient is significant since the turbine speed is much increased due to the low inertia of the wind turbine simulator. Fig. 16(h) shows the dc-link voltage response, where the maximum voltage variation at the transient state is about 7%.

Fig. 17 shows the comparison of the responses for the two dc-link voltage controllers: 1) for the conventional PI controllers, $k_P = 0.235$ and $k_I = 13.298$, and 2) for the feedback linearization method, $k_1 = 0.249$ and $k_2 = 1.408$ ($s_{1,2} = -75 \pm j50$). It is obvious that the proposed method gives faster response and lower overshoot than the conventional PI controllers.

## VII. Conclusion

This paper has proposed an LVRT strategy of the variable speed wind turbine using PMSGs for the grid voltage sags.

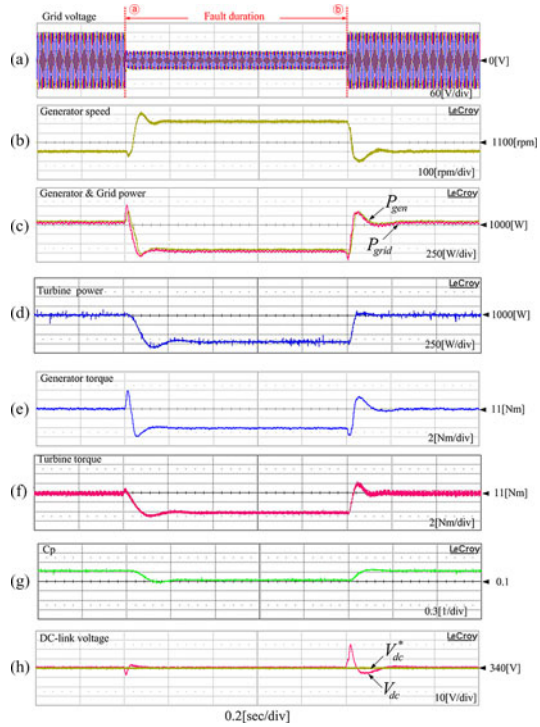


Fig. 16. System performance under three-phase balanced voltage sag. (a) Grid voltage. (b) Generator speed. (c) Generator and grid power. (d) Turbine power. (e) Generator torque. (f) Turbine torque. (g) Power conversion coefficient. (h) DC-link voltage.

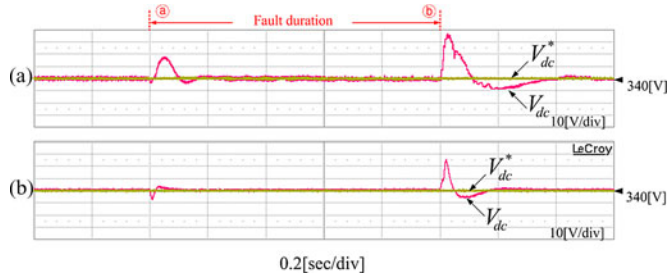


Fig. 17. Performance of dc-link voltage control. (a) PI control. (b) Feedback linearization.

In this method, the dc-link voltage control is performed by the generator-side converter, not by the GSC which is usually used. A new dc-link voltage controller has been designed and implemented using feedback linearization theory. The GSC controls the grid power according to the MPPT strategy. For unbalanced grid voltage conditions, the current control using a double-frame controller has been applied for the positive- and negative-sequence components. The validity of the control algorithm has been verified by simulation results for a 2 MW PMSG wind power system. Also, experimental verification has been done for a 2.68 kW PMSG wind turbine simulator. The test results have shown a good dc-link voltage control performances for unbalanced grid voltage sags.

## References

[1] M. Chinchilla, S. Arnaltes, and J. C. Burgos, "Control of permanent-magnet generators applied to variable-speed wind-energy systems connected to the grid," *IEEE Trans. Energy Convers.*, vol. 21, no. 1, pp. 130–135, Mar. 2006.

[2] H. Polinder, F. F. A van der Pijl, and P. Tavner, "Comparison of direct-drive and geared generator concepts for wind turbines," *IEEE Trans. Energy Convers.*, vol. 21, no. 3, pp. 543–550, Sep. 2006.
[3] F. Iov, A. D. Hansen, P. Sørensen, and N. A. Cutululis, "Mapping of grid faults and grid codes," Risø Nat. Lab., Tech. Univ. Denmark, Roskilde, Denmark, Tech. Rep. Risø-R-1617(EN), Jul. 2007.
[4] C. Saniter and J. Janning, "Test bench for grid code simulations for multi-MW wind turbines, design and control," *IEEE Trans. Power Electron.*, vol. 23, no. 4, pp. 1707–1715, Jul. 2008.
[5] J.-H. Jeon, S.-K. Kim, C.-H. Cho, J.-B. Ahn, and E.-S. Kim, "Development of simulator system for micro-grids with renewable energy sources," *J. Electr. Eng. Technol.*, vol. 1, no. 4, pp. 409–413, Feb. 2006.
[6] R. Pollin, H. G. Peltier, and H. Scharber, "Green recovery: A new program to create good jobs and start building a low-carbon economy," Center for American Progress, Washington, DC, Sep. 2008. Available: http://www.peri.umass.edu/fileadmin/pdf/other_publication_types/green_economics/peri_report.pdf.
[7] F. K. A. Lima, A. Luna, P. Rodriguez, E. H. Watanabe, and F. Blaabjerg, "Rotor voltage dynamics in the doubly fed induction generator during grid faults," *IEEE Trans. Power Electron.*, vol. 25, no. 1, pp. 118–130, Jan. 2010.
[8] L. G. Meegahapola, T. Littler, and D. Flynn, "Decoupled-DFIG fault ride-through strategy for enhanced stability performance during grid faults," *IEEE Trans. Sustainable Energy*, no. 3, pp. 152–162, Oct. 2010.
[9] Q. Song and W. Liu, "Control of a cascade STATCOM with star configuration under unbalanced conditions," *IEEE Trans. Power Electron.*, vol. 24, no. 1, pp. 45–58, Jan. 2009.
[10] W. H. Zhang, S.-J. Lee, and M.-S. Choi, "Setting considerations of distance relay for transmission line with STATCOM," *J. Electr. Eng. Technol.*, vol. 5, no. 4, pp. 522–529, Jul. 2010.
[11] H. M. Pirouzy and M. T. Bina, "Modular multilevel converter based STATCOM topology suitable for medium-voltage unbalanced systems," *J. Power Electron.*, vol. 10, no. 5, pp. 572–578, Sep. 2010.
[12] G. Brando, A. Coccia, and R. Rizzo, "Control method of a braking chopper to reduce voltage unbalance in a 3-level chopper," in *Proc. IEEE Int. Conf. Ind. Technol.*, 2004, vol. 2, pp. 975–978.
[13] J. F. Conroy and R. Watson, "Low-voltage ride-through of a full converter wind turbine with permanent magnet generator," *IET Renewable Power. Generation*, vol. 1, no. 3, pp. 182–189, Sep. 2007.
[14] W. Li, C. Abbey, and G. Joos, "Control and performance of wind turbine generators based on permanent magnet synchronous machines feeding a diode rectifier," in *Proc. IEEE Power Electron. Spec. Conf.*, Jun., 2006, pp. 1–6.
[15] B. Singh, R. Saha, A. Chandra, and K. Al-Haddad, "Static synchronous compensators (STATCOM): A review," *IET Power Electron.*, vol. 2, no. 4, pp. 297–324, 2009.
[16] A. D. Hansen and G. Michalke, "Multi-pole permanent magnet synchronous generator wind turbines' grid support capability in uninterrupted operation during grid faults," *IET Renewable Power Generation*, vol. 3, no. 3, pp. 333–348, 2009.
[17] X. Yuan, F. Wang, D. Boroyevich, Y. Li, and R. Burgos, "DC-link voltage control of a full power converter for wind generator operating in weak-grid systems," *IEEE Trans. Power Electron.*, vol. 24, no. 9, pp. 2178–2192, Sep. 2009.
[18] D.-C. Lee, G.-M. Lee, and K.-D. Lee, "DC-bus voltage control of three-phase ac/dc PWM converters using feedback linearization," *IEEE Trans. Ind. Appl.*, vol. 36, no. 3, pp. 826–833, May 2000.
[19] D.-E. Kim and D.-C. Lee, "Feedback linearization control of three-phase UPS inverter systems," *IEEE Trans. Ind. Electron.*, vol. 57, no. 3, pp. 963–968, Mar. 2010.
[20] K.-H. Kim, Y.-C. Jeung, D.-C. Lee, and H.-G. Kim, "Robust control of PMSG wind turbine systems with back-to-back PWM converters," in *Proc. IEEE Int. Symp. Power Electron. Distrib. Generation*, 2010, pp. 433–437.
[21] A. Miller, E. Muljadi, and D. S. Zinger, "A variable speed wind turbine power control," *IEEE Trans. Energy Convers.*, vol. 12, no. 2, pp. 181–186, Jun. 1997.
[22] M. Singh and A. Chandra, "Application of adaptive network-based fuzzy inference system for sensorless control of PMSG-based wind turbine with nonlinear-load-compensation capabilities," *IEEE Trans. Power Electron.*, vol. 26, no. 1, pp. 165–175, Jan. 2011.
[23] T. H. Nguyen, S.-H. Jang, H.-G. Park, and D.-C. Lee, "Sensorless control of PM synchronous generators for micro wind turbines," in *Proc. IEEE 2nd Int. Power Energy Conf.*, Dec. 2008, pp. 936–941.
[24] J. Dai, D. Xu, B. Wu, and N. R. Zargari, "Unified DC-link current control for low-voltage ride-through in current-source-converter-based wind energy conversion systems," *IEEE Trans. Power Electron.*, vol. 26, no. 1, pp. 288–297, Jan. 2011.
[25] G. Foo and M. F. Rahman, "Sensorless direct torque and flux-controlled IPM synchronous motor drive at very low speed without signal injection," *IEEE Trans. Power Electron.*, vol. 57, no. 1, pp. 395–403, Jan. 2010.
[26] J. J. E. Slotine and W. Li, *Applied Nonlinear Control*. Englewood Cliffs, NJ: Prentice-Hall, 1991, pp. 207–271.
[27] G.-M. Lee, D.-C. Lee, and J.-K. Seok, "Control of series active power filters compensating for source voltage unbalance and current harmonics," *IEEE Trans. Ind. Appl.*, vol. 51, no. 1, pp. 132–139, Feb. 2004.
[28] H.-S. Song and K. Nam, "Dual current control scheme for PWM converter under unbalanced input voltage conditions," *IEEE Trans. Ind. Appl.*, vol. 46, no. 5, pp. 953–959, Oct. 1999.
[29] S.-K. Sul, *Control of Electric Machine Drive System*. Piscataway, NJ: IEEE Press, 2011.
[30] C. T. Chen, *Linear System Theory and Design*. New York: Oxford Univ. Press, 1999.

**Ki-Hong Kim** was born in 1982. He received the B.S. and M.S. degrees in electrical engineering from Yeungnam University, Gyeongsan, Korea, in 2008 and 2011, respectively.

He is currently with LG Electronics Inc., Changwon, Korea. His research interests include control of power converters, renewable energy systems, and motor drives.

**Yoon-Cheul Jeung** was born in 1985. He received the B.S. degree in electrical engineering from Yeungnam University, Gyeongsan, Korea, in 2010, where he is currently working toward the M.S. degree at the Power Electronics and Machine Control Laboratory.

His research interests include control of power converters, battery charger, and power quality.

**Dong-Choon Lee** (S'90–M'95) received the B.S., M.S., and Ph.D. degrees in electrical engineering from Seoul National University, Seoul, Korea, in 1985, 1987, and 1993, respectively.

From 1997 to 1998, he was a Research Engineer with Daewoo Heavy Industry. Since 1994, he has been a faculty member in the Department of Electrical Engineering, Yeungnam University, Gyeongbuk, Korea, where he is currently a Full Professor. As a Visiting Scholar, he joined Power Quality Laboratory, Texas A&M University, College Station, in 1998, Electrical Drive Center, University of Nottingham, U.K., in 2001, and Wisconsin Electric Machines & Power Electronic Consortium, University of Wisconsin, Madison, in 2004. His research interests include ac machine drives, control of power converters, wind power generation, and power quality.

Dr. Lee is serving as a Publication Editor for *Journal of Power Electronics*, the Korean Institute of Power Electronics, Korea.

**Heung-Geun Kim** (S'82–M'85) was born in Korea in 1956. He received the B.S., M.S., and Ph.D. degrees in electrical engineering from Seoul National University, Seoul, Korea, in 1980, 1982, and 1988, respectively.

Since 1984, he has been with the Department of Electrical Engineering, Kyungpook National University, Daegu, Korea, where he is currently a Full Professor and the Director of Microgrid Research Center. From 1990 to 1991, he was a Visiting Scholar in the Department of Electrical Engineering, the University of Wisconsin-Madison, Madison. From 2006 to 2007, he served as a Visiting Scholar in the Department of Electrical and Computer Engineering, Michigan State University, East Lansing. His current research interests include control of ac machines, photovoltaic power generation, and microgrid system.